ORGANOMETALLICS

pubs.acs.org/Organometallics Article

Coordination-Induced N−H Bond Weakening in a Molybdenum Pyrrolidine Complex: Isotopic Labeling Provides Insight into the Pathway for H_2 Evolution

Máté J. Bezdek, István Pelczer, and Paul J. Chirik*

Cite This: https://dx.doi.org/10.1021/acs.organomet.0c00471 Read Online

ACCESS | Metrics & More | Article Recommendations | Supporting Information

ABSTRACT: The synthesis and characterization of a cationic molybdenum pyrrolidine complex are described that exhibits significant coordination-induced N−H bond weakening. The N−H bond dissociation free energy (BDFE) of the coordinated pyrrolidine in $[(^{Ph}Tpy)(PPh_2Me)_2Mo(NH(pyrr))][BArF^{24}]$ ($[\mathbf{1\text{-}NH(pyrr)}]^+$; ^{Ph}Tpy = 4′-Ph-2,2′,6′,2″-terpyridine, NH(pyrr) = pyrrolidine, ArF^{24} = $[C_6H_3\text{-}3,5\text{-}(CF_3)_2]_4$) was determined to be between 41 and 51 kcal mol^{-1} by thermochemical analysis and supported by a density functional theory (DFT) computed value of 48 kcal mol^{-1}. The complex $[\mathbf{1\text{-}NH(pyrr)}]^+$ underwent proton-coupled electron transfer (PCET) to 2,4,6-tri-*tert*-butylphenoxyl radical, as well as spontaneous H_2 evolution upon gentle heating to furnish the corresponding molybdenum pyrrolidide complex $[(^{Ph}Tpy)(PPh_2Me)_2Mo(N(pyrr))][BArF^{24}]$ ($[\mathbf{1\text{-}N(pyrr)}]^+$). Thermolysis of the deuterated isotopologue $[\mathbf{1\text{-}ND(pyrr)}]^+$ still produced H_2 with concomitant incorporation of the isotopic label into the pyrrolidide ligand in the product $[(\mathbf{1\text{-}N(pyrr\text{-}}d_n\mathbf{)})]^+$ (n = 0−2), consistent with an H_2 evolution pathway involving *intra*molecular H−H bond formation followed by an *inter*molecular product-forming PCET step. These observations provide the context for understanding H_2 evolution in the nonclassical ammine complex $[(^{Ph}Tpy)(PPh_2Me)_2Mo(NH_3)][BArF^{24}]$ ($[\mathbf{1\text{-}NH_3}]^+$) and are supported by DFT-computed reaction thermochemistry. Overall, these studies offer rare insight into the H_2 formation pathway in nonclassical amine complexes with N−H BDFEs below the thermodynamic threshold for H_2 evolution and inform the development of well-defined, thermodynamically potent PCET reagents.

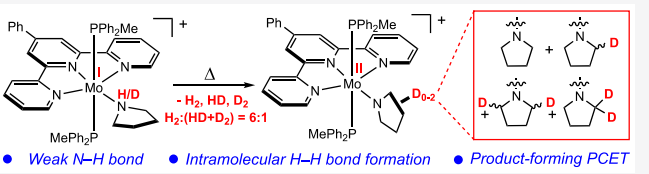

INTRODUCTION

Coordination of a ligand to a transition metal, a foundational principle in inorganic chemistry, fundamentally alters the bonding properties of the ligand including lowering the homolytic X−H (X = C, N, O) bond dissociation free energies (BDFEs).[1] Termed coordination-induced bond weakening, this phenomenon is key to understanding the thermochemistry of proton-coupled electron transfer (PCET) processes[2−4] in transition-metal complexes and has implications in biology,[5−7] organic synthesis[8,9] as well as energy science.[10−12] In contrast to the extensive thermochemical data available for organic molecules, systematic reports of analogous BDFE data for ligand X−H bonds (X = C, metal, N, O, P) have only recently emerged and remain scarce by comparison.[1,13−17]

In rare instances, coordination-induced bond weakening has been demonstrated or proposed to have a dramatic impact on X−H BDFEs that are quantified in terms of a 1e$^-$ redox couple ($E°$), X−H pK_a, and the solvent-specific H^+ standard reduction potential (C_G; eq 1):[18]

$$\mathrm{BDFE_{X-H}} = 1.37\mathrm{p}K_a + 23.06E° + C_G \quad (1)$$

Metal−ligand combinations with low X−H BDFEs are desirable in synthetic chemistry with application as potent H atom donors to enable reductive PCET with substrates such as epoxides, olefins, and enamines.[8,9] For instance, Cuerva[19,20] and later Gansäuer[21] demonstrated that $(\eta^5\text{-}C_5H_5)_2TiCl_2$, in combination with a manganese reductant in THF/water mixtures, forms $[(\eta^5\text{-}C_5H_5)_2Ti(H_2O)_m(THF)_n]^+$ complexes and promote the reductive ring opening of epoxides enabled by the O−H bond weakening in water by over 60 kcal mol^{-1} (Scheme 1a, left). Similarly, Flowers[22] and Mayer[23] reported that $SmI_2(H_2O)_n$ mixtures are effective for achieving thermodynamically challenging reductions of anthracene and enamines, respectively, with an estimated O−H BDFE of 26 kcal mol^{-1} resulting from the coordination of H_2O to samarium(II) (Scheme 1a, right). Recently, Nishibayashi applied $SmI_2(H_2O)_n$ to catalytic nitrogen fixation, where $SmI_2(H_2O)_n$ was used to deliver H atom equivalents to a reduced molybdenum dinitrogen precatalyst, ultimately furnishing free ammonia.[24] Interest therefore remains in the development of well-defined, yet thermodynamically potent PCET reagents with low X−H BDFEs.

Received: July 11, 2020

Scheme 1

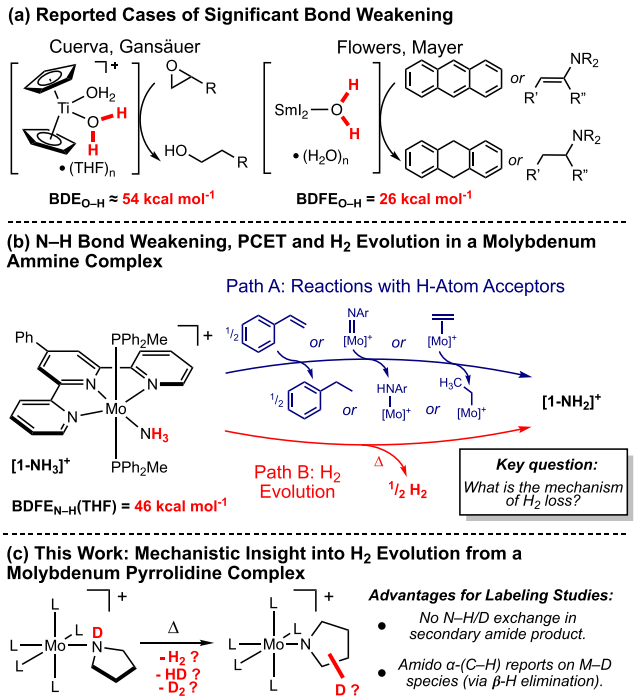

Our laboratory recently reported the synthesis of an isolable nonclassical ammine complex, [(^{Ph}Tpy)(PPh$_2$Me)$_2$Mo(NH$_3$)][BArF^{24}] ([**1-NH$_3$**]$^+$; ^{Ph}Tpy = 4′-Ph-2,2′,6′,2″-terpyridine, ArF^{24} = [C$_6$H$_3$-3,5-(CF$_3$)$_2$]$_4$), that exhibits a remarkably low N−H BDFE of 46 kcal mol^{-1} in the coordinated ammonia, below the thermodynamic threshold for spontaneous hydrogen evolution (ΔG_f°(H$^\bullet$) = 49 kcal mol^{-1}, gas phase).[25] The ammine complex [**1-NH$_3$**]$^+$ is a competent PCET reagent that has been shown to deliver H atom equivalents to acceptors such as styrene as well as the molybdenum imido and ethylene complexes [(^{Ph}Tpy)(PPh$_2$Me)$_2$Mo(N*t*BuAr)][BArF^{24}] ([**1-(N*t*BuAr)**]$^+$; *t*BuAr = 4-*tert*-butyl-C$_6$H$_4$) and [(^{Ph}Tpy)(PPh$_2$Me)$_2$Mo(C$_2$H$_4$)][BArF^{24}] ([**1-(C$_2$H$_4$)**]$^+$), to furnish ethylbenzene or the corresponding molybdenum amido and ethyl complexes [**1-(NH*t*BuAr)**]$^+$ and [**1-(CH$_2$CH$_3$)**]$^+$, respectively (Scheme 1b, Path A).[26,27] In contrast to SmI$_2$(H$_2$O)$_n$, mild thermolysis of [**1-NH$_3$**]$^+$ at 60 °C resulted in H$_2$ evolution with concomitant generation of the corresponding molybdenum amido complex [**1-NH$_2$**]$^+$ (Scheme 1b, Path B). While thermochemical studies suggest that PCET from [**1-NH$_3$**]$^+$ occurs either by electron transfer followed by proton transfer or by a concerted pathway,[26,27] to date there has been little experimental study into the pathway for H$_2$ evolution. Gaining insight into the mechanism of H$_2$ loss from [**1-NH$_3$**]$^+$ is therefore of interest to guide the development of kinetically stable yet thermodynamically potent PCET reagents as well as to provide design principles for bond activation in the context of NH$_3$ oxidation[13,28−36] and catalysis involving metal−ligand cooperation.[37−39]

Following the discovery of [**1-NH$_3$**]$^+$, important questions immediately arose concerning the molecularity of the H$_2$ evolution step. While attempts were made to address this question with deuterium-labeling experiments, the exchangeable N−H bonds present in both the molybdenum ammine starting material and amido product complicated an interpretation of the results.[25] Coordination of a secondary amine would eliminate this competing process, as the resulting N,N-dialkyl amide lacks a site for exchange (Scheme 1c). Pyrrolidine was selected as a representative secondary amine, as coordination to the cationic terpyridine bis(phosphine) molybdenum(I) complex would likely result in N−H bond weakening on the order of that observed for ammonia and should give rise to analogous H$_2$ evolution to yield the corresponding secondary alkyl amido product (Scheme 1c). In addition, pyrrolidide α-(C−H) bonds are well poised to undergo β-H elimination, thereby reporting on potential Mo−D intermediates generated during dehydrogenation.

Here we describe the synthesis and characterization of the targeted cationic molybdenum pyrrolidine complex [(^{Ph}Tpy)(PPh$_2$Me)$_2$Mo(NH(pyrr))][BArF^{24}] ([**1-NH(pyrr)**]$^+$; NH(pyrr) = pyrrolidine) and explore its electronic structure, thermochemical properties, and H$_2$ evolution reactivity. Deuterium labeling studies with the N−D isotopologue are reported that provide insight into the H$_2$ evolution pathway in [**1-NH(pyrr)**]$^+$ and provide a context for understanding the dehydrogenation reactivity of the related ammine complex [**1-NH$_3$**]$^+$.

RESULTS AND DISCUSSION

Synthesis and Characterization of the Molybdenum Pyrrolidine Complex [1-NH(pyrr)]$^+$. Our studies commenced with the synthesis of the terpyridine bis(phosphine) molybdenum pyrrolidine complex [**1-NH(pyrr)**]$^+$. Stirring a benzene solution containing [(^{Ph}Tpy)(PPh$_2$Me)$_2$MoCl] ([**1-Cl**])[40] and 1 equiv of both Na[BArF^{24}] and pyrrolidine at room temperature for 18 h furnished a dark green solid in 85% yield identified as [**1-NH(pyrr)**]$^+$ (Figure 1a). The solid-state infrared spectrum (KBr) of [**1-NH(pyrr)**]$^+$ exhibits an isotopically sensitive N−H vibration at 3246 cm^{-1} that shifts to 2400 cm^{-1} in the d_1 isotopologue [**1-ND(pyrr)**]$^+$, consistent with the coordination of pyrrolidine upon chloride

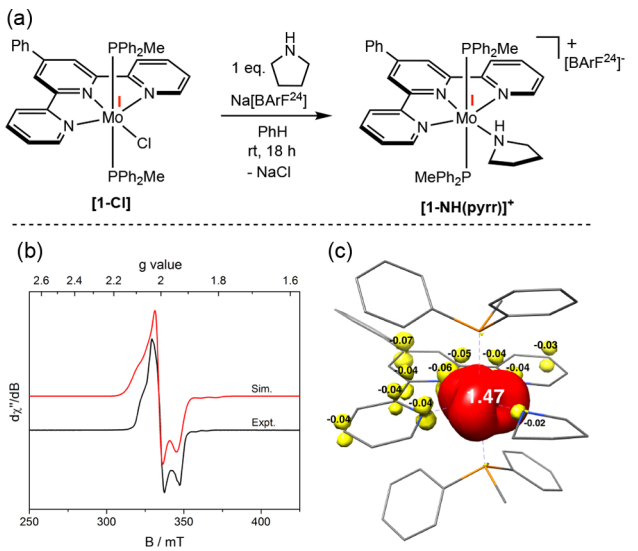

Figure 1. (a) Synthesis of [**1-NH(pyrr)**]$^+$ by chloride abstraction. (b) X-band EPR spectrum of [**1-NH(pyrr)**]$^+$ recorded in toluene glass at 8 K. Collection and simulation parameters: microwave frequency 9.381 GHz, power 2.0 mW, modulation amplitude 4.0 G; g_x = 2.020, g_y = 2.005, g_z = 1.968. (c) DFT-computed spin density plot for [**1-NH(pyrr)**]$^+$ obtained from Mulliken population analysis in the gas phase at the B3LYP level of theory.

https://dx.doi.org/10.1021/acs.organomet.0c00471
Organometallics XXXX, XXX, XXX−XXX

abstraction. The formally Mo(I) complex [**1-NH(pyrr)**]$^+$ has an $S = 1/2$ ground state, as evidenced by a solid-state magnetic moment of 1.7(2) μ_B (Guoy balance, 23 °C). The EPR spectrum of [**1-NH(pyrr)**]$^+$ was collected in toluene glass at 8 K and exhibits a rhombic signal that was readily simulated with the g values $g_x = 2.020$, $g_y = 2.005$, and $g_z = 1.968$ (Figure 1b). This EPR spectrum closely resembles the rhombic signal observed for [**1-NH$_3$**]$^+$ at 7 K (see the Supporting Information), suggesting that the electronic structures of the parent ammine and pyrrolidine complexes are analogous. Accordingly, the DFT-computed Mulliken spin density plot for [**1-NH(pyrr)**]$^+$ supports a molybdenum-centered singly occupied molecular orbital (SOMO, Figure 1c) in agreement with the electronic structure previously determined for [**1-NH$_3$**]$^+$.[25]

Determination of the N−H BDFE of Coordinated Pyrrolidine in [1-NH(pyrr)]$^+$. Efforts were next directed at experimentally establishing the N−H BDFE in [**1-NH(pyrr)**]$^+$. Homolytic cleavage of the pyrrolidine N−H bond in [**1-NH(pyrr)**]$^+$ was accomplished by addition of 1 equiv of 2,4,6-tri-*tert*-butylphenoxyl radical (tBu$_3$ArO$^\bullet$) to generate the diamagnetic molybdenum(II) pyrrolidide complex [(^{Ph}Tpy)-(PPh$_2$Me)$_2$Mo(NC$_4$H$_8$)][BArF^{24}] ([**1-N(pyrr)**]$^+$) in quantitative yield within 30 min at room temperature (Scheme 2a, top). The benzene-d_6 ^{1}H NMR spectrum of [**1-N(pyrr)**]$^+$ exhibits the number of resonances consistent with a C_{2v}-symmetric molecule in solution with diagnostic pyrrolidide α- and β-(C−H) signals at 4.04 and 1.75 ppm, respectively, and a single ^{31}P{^{1}H} peak at 11.95 ppm that is consistent with *trans*-PPh$_2$Me ligands coordinated to cationic molybdenum(II) amido.[25,26] While the H atom abstraction reactivity with tBu$_3$ArO$^\bullet$ establishes the upper bound of the N−H BDFE in [**1-NH(pyrr)**]$^+$ as that of the O−H bond in tBu$_3$ArOH (77 kcal mol^{-1}),[41] the pyrrolidide product [**1-N(pyrr)**]$^+$ was also accessed by thermal dehydrogenation of the pyrrolidine complex (Scheme 2a, bottom). Heating a benzene-d_6 solution of [**1-NH(pyrr)**]$^+$ at 60 °C for 48 h furnished [**1-N(pyrr)**]$^+$ in 98% yield with the concomitant formation of H_2, as confirmed by Toepler pump experiments (81% yield of H_2). The spontaneous dehydrogenation reactivity observed[42] establishes the upper bound of the N−H BDFE in [**1-NH(pyrr)**]$^+$ as the free energy of H$^\bullet$ formation from H_2 in benzene solution (∼51 kcal mol^{-1}).[1]

Scheme 2. Synthesis of [1-N(pyrr)]$^+$ and Thermochemical Square Scheme Defining the N−H BDFE in [1-NH(pyrr)]$^+$

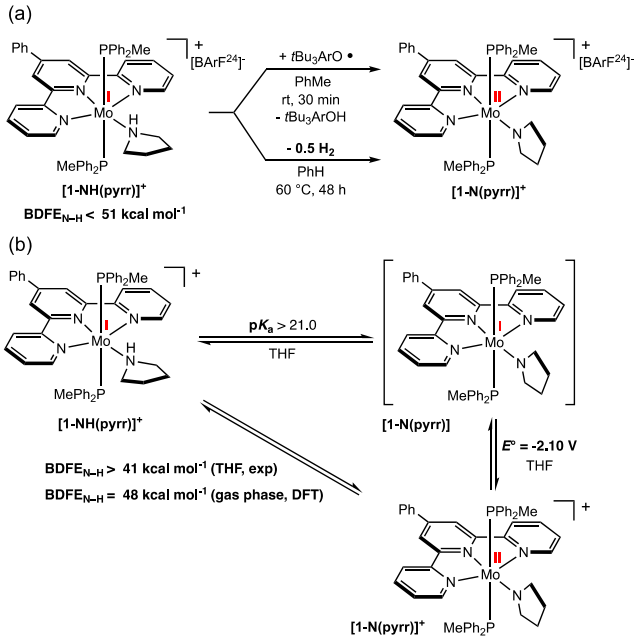

The low upper bound for the N−H BDFE in [**1-NH(pyrr)**]$^+$ complicates an estimation of its absolute value, given the lack of reference reagents near the thermodynamic threshold for H_2 evolution. Therefore, the N−H BDFE was instead estimated using a thermochemical square scheme (Scheme 2b). Because the electrochemistry of [**1-NH(pyrr)**]$^+$ proved intractable, the cyclic voltammogram of [**1-N(pyrr)**]$^+$ was collected to probe the thermodynamics of accessing the one-electron-reduced pyrrolidide complex [**1-N(pyrr)**] that in turn enables estimation of the $E°$ and pK_a terms in Scheme 2b. The cyclic voltammogram (CV) of [**1-N(pyrr)**]$^+$ was collected in THF solution and exhibits two reversible anodic waves with $E_{1/2} = -0.63$ and 0.08 V vs Fc/Fc$^+$ (Fc = [Cp$_2$Fe]) assignable to oxidations to yield [**1-N(pyrr)**]$^{2+}$ and [**1-N(pyrr)**]$^{3+}$, respectively (Figure 2, black trace). In addition, a quasi-reversible cathodic wave was observed in the CV of [**1-N(pyrr)**]$^+$ at $E_{1/2} = -2.10$ V that corresponds to a reduction to yield the neutral pyrrolidide complex [**1-N(pyrr)**] and was of interest for estimating the N−H BDFE in [**1-NH(pyrr)**]$^+$.

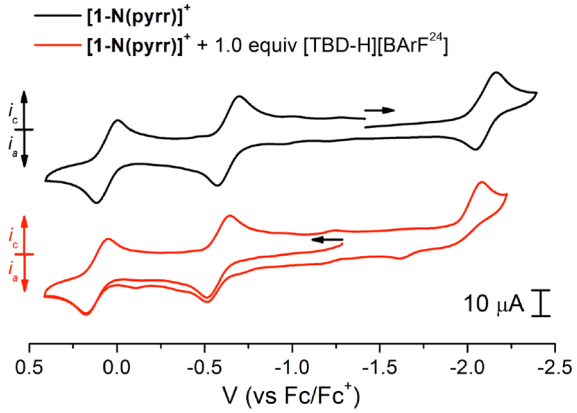

Figure 2. Cyclic voltammograms of [**1-N(pyrr)**]$^+$ (2.0 mM in THF, black trace) and [**1-N(pyrr)**]$^+$ in the presence of 1.0 equiv of [TBD-H][BArF^{24}] (2.0 mM, red trace) using a glassy-carbon working electrode, a platinum-wire counter electrode, a silver-wire reference electrode, 0.2 M [(n-Bu)$_4$N][PF$_6$], and a scan rate of 100 mV s^{-1} in THF at 23 °C versus Fc/Fc$^+$. TBD = triazabicyclodecene.

Attempts to synthesize [**1-N(pyrr)**] by one-electron reduction of [**1-N(pyrr)**]$^+$ afforded intractable product mixtures, and as a result, the lower bound for the pK_a of [**1-NH(pyrr)**]$^+$ was estimated by *in situ* protonation experiments in the electrochemical cell. Upon collection of the CV of [**1-N(pyrr)**]$^+$ in the presence of 1 equiv of [TBDH][BArF^{24}] (TBD = triazabicyclodecene), the cathodic wave became irreversible with a concomitant positive shift of the peak cathodic potential from $E_{pc} = -2.17$ V (no [TBDH][BArF^{24}]) to −2.13 V (1.0 equiv of [TBDH][BArF^{24}]) (Figure 2, red trace). These observations are consistent with an EC mechanism involving fast electron transfer (E) followed by rate-limiting proton transfer (C) from [TBDH][BArF^{24}] to *in situ* generated [**1-N(pyrr)**].[43,44] Evaluation of the peak potential as a function of added acid allowed the determination

https://dx.doi.org/10.1021/acs.organomet.0c00471
Organometallics XXXX, XXX, XXX−XXX

of the bimolecular proton transfer rate constant as k_{PT} = 1.3 × 10^3 M^{-1} s^{-1}, a rare quantification of amido ligand protonation kinetics (Figure 3; see the Supporting Information for

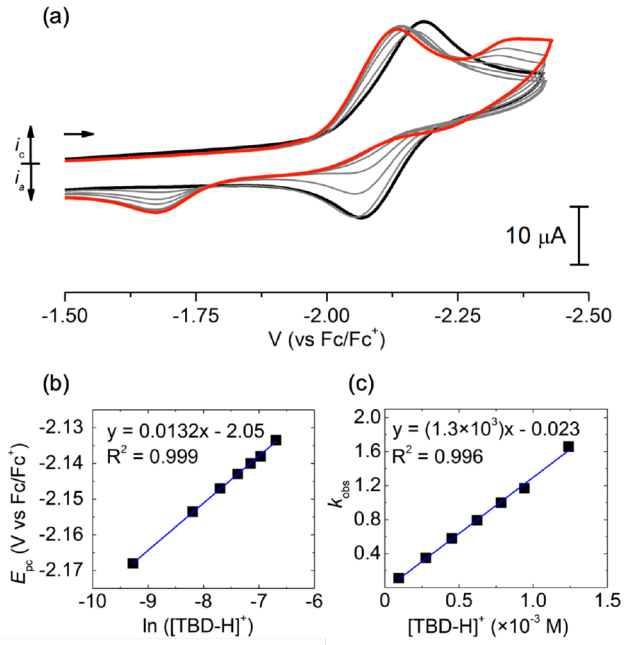

Figure 3. (a) Cyclic voltammograms of [**1-N(pyrr)**]$^+$ (2.0 mM in THF) in the presence of 0 M (black trace) to 1.2 mM (red trace) of [TBD-H][$BArF^{24}$] using a glassy-carbon working electrode, a platinum-wire counter electrode, a silver-wire reference electrode, 0.2 M [nBu_4N][PF_6], and a scan rate of 100 mV s^{-1} in THF at 23 °C versus Fc/Fc^+. (b) Plot of peak cathodic potential (E_{pc}) for the [**1-N(pyrr)**]$^+$/[**1-N(pyrr)**] wave as a function of ln([TBD-H]$^+$). The slope is equal to 0.0132 with R^2 = 0.999. (c) Plot of k_{obs} obtained as a function of [TBD-H]$^+$ concentration. The slope yields k_{PT} = 1.3 × 10^3 M^{-1} s^{-1} with R^2 = 0.996.

derivation). While the quasi-reversibility of the cathodic wave in [**1-N(pyrr)**]$^+$ precludes the extraction of equilibrium parameters for the EC reaction, the observation of the rapid protonation of *in situ* generated [**1-N(pyrr)**] by the weak acid [TBDH][$BArF^{24}$] implies that the pK_a of this acid (21.0 in THF)[45] is likely a satisfactory lower bound for the pK_a of [**1-NH(pyrr)**]$^+$.[46] These data, in combination with the $E°$ value for the [**1-N(pyrr)**]$^+$/[**1-N(pyrr)**] couple ($E_{1/2}$ = −2.10 V), define the lower bound for the N−H BDFE in [**1-NH(pyrr)**]$^+$ as 41 kcal mol^{-1} in THF according to eq 1.[47,48] Together with the observation of spontaneous H_2 evolution from the complex, an experimental bound for the N−H BDFE of 41−51 kcal mol^{-1} is obtained for [**1-NH(pyrr)**]$^+$, in close agreement with a DFT-computed value of 48 kcal mol^{-1} (gas phase). These data establish [**1-NH(pyrr)**]$^+$ as a rare example of a nonclassical amine complex that is thermodynamically unstable with respect to H_2 evolution.

Isotopic Labeling Experiments. We next turned our attention to deuterium labeling experiments to gain insight into the pathway of H_2 evolution from [**1-NH(pyrr)**]$^+$. Mildly heating the ND isotopologue [**1-ND(pyrr)**]$^+$ at 60 °C for 48 h and analyzing the evolved gases by ^{1}H NMR spectroscopy revealed the generation of H_2 and HD gases in a 9:1 ratio. To probe the amount of D_2 formed, the evolved gases were passed over CuO at 200 °C for 30 min, collected, and analyzed as the isotopologues of H_2O. Unlike the nonexchangeable isotopologues of H_2, rapid H/D exchange equilibrates protons and deuterons in the water product and the resulting H_2O:HDO ratio is expected to reflect the overall deuterium content, including D_2. Accordingly, the ^{1}H NMR spectrum of the combustion product established a H_2O:HDO ratio of 6:1 and therefore an overall H_2:(HD + D_2) ratio of 6:1 prior to combustion (Figure S12; see the Supporting Information for experimental details). Importantly, these results demonstrate that <5% of D_2 is evolved during the dehydrogenation of [**1-ND(pyrr)**]$^+$ and imply substantial deuterium incorporation in the molybdenum pyrrolidide product denoted as [**1-N(pyrr-d_n)**]$^+$ in Figure 4a.

To determine the fate of the deuterium label following dehydrogenation of [**1-ND(pyrr)**]$^+$, the quantification and location of the deuterium content in the molybdenum pyrrolidide product [**1-N(pyrr-d_n)**]$^+$ was pursued. Notably, the ^{2}H NMR spectrum of [**1-N(pyrr-d_n)**]$^+$ established significant deuterium incorporation in the α-pyrrolidide

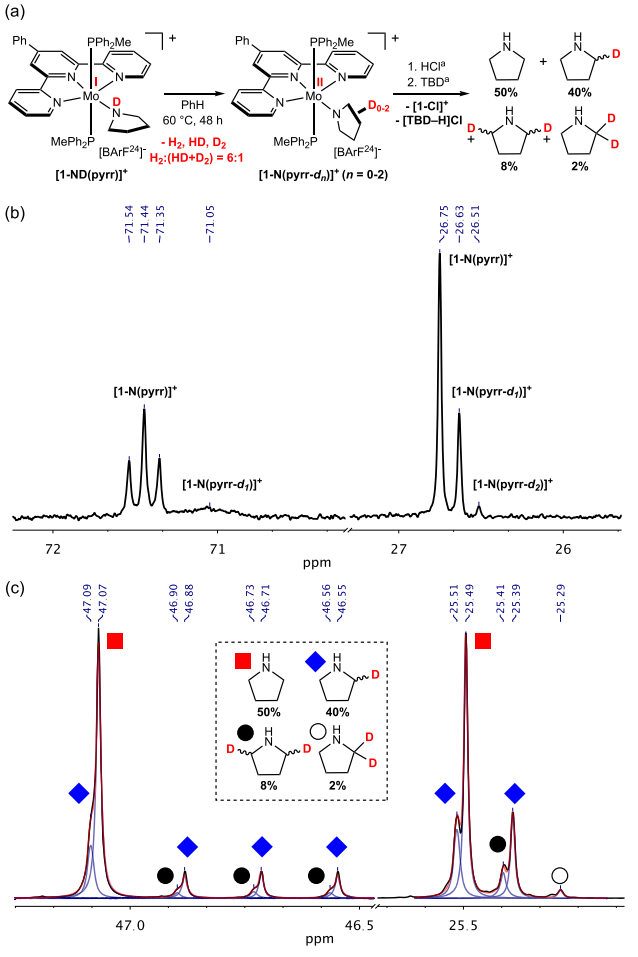

Figure 4. (a) Isotope labeling experiment and pyrrolidide ligand liberation in [**1-N(pyrr-d_n)**]$^+$. Legend: (a) for the reaction conditions, see the Supporting Information. (b) Pyrrolidide α- and β-carbon region of the $^{13}C\{^1H\}$ NMR spectrum (benzene-d_6, 23 °C) of [**1-N(pyrr-d_n)**]$^+$ exhibiting isotopic perturbation of the resonances. (c) Quantitative $^{13}C\{^1H\}$ NMR spectrum (benzene-d_6, 23 °C) of a mixture containing pyrrolidine (50%), pyrrolidine-2-d_1 (40%), pyrrolidine-2,5-d_2 (8%) and pyrrolidine-2-d_2 (2%) liberated from [**1-N(pyrr-d_n)**]$^+$ by protonolysis. The red symbols represent a fit of the data, and the blue symbols show the deconvolution of the individual peaks.

https://dx.doi.org/10.1021/acs.organomet.0c00471
Organometallics XXXX, XXX, XXX−XXX

position (4.04 ppm), corroborated by $^{13}C\{^1H\}$ NMR spectroscopy, which revealed an isotopic perturbation of both α- and β-pyrrolidide carbon resonances. In addition to the expected triplet for the α-pyrrolidine carbons in $[\mathbf{1\text{-}N(pyrr)}]^+$ at 71.44 ppm ($^3J_{C-P}$ = 11.6 Hz), a broad peak was observed at 71.05 ppm that corresponds to a deuterated α-pyrrolidide carbon in $[\mathbf{1\text{-}N(pyrr\text{-}}d_1\mathbf{)}]^+$ that is broadened due to coupling to deuterium as well as two equivalent phosphorus atoms in the *trans*-PPh_2Me ligands (Figure 4b). Additionally, three distinct singlets were observed at 26.75, 26.63, and 26.51 ppm corresponding to the pyrrolidide β-carbon signals of $[\mathbf{1\text{-}N(pyrr)}]^+$, $[\mathbf{1\text{-}N(pyrr\text{-}}d_1\mathbf{)}]^+$ and $[\mathbf{1\text{-}N(pyrr\text{-}}d_2\mathbf{)}]^+$, respectively, with isotopic shifts arising due to remote deuteration at the α-pyrrolidide carbon (Figure 4b).

Because coupling to the two equivalent phosphorus atoms in PPh_2Me ligands complicated the assignment and quantification of the pyrrolidide isotopomers and isotopologues present in $[\mathbf{1\text{-}N(pyrr\text{-}}d_n\mathbf{)}]^+$, the pyrrolidide ligand was liberated from the coordination sphere of molybdenum by protonolyis and analyzed as free pyrrolidine. Accordingly, treatment of $[\mathbf{1\text{-}N(pyrr\text{-}}d_n\mathbf{)}]^+$ with excess HCl generated $[(^{Ph}Tpy)(PPh_2Me)_2Mo(Cl)][BArF^{24}]$ ($[\mathbf{1\text{-}Cl}]^+$) and pyrrolidinium-d_n chloride (n = 0−2), as judged by ^1H NMR spectroscopy. Further treatment of the reaction mixture with the base TBD and vacuum transfer of the volatiles enabled exclusive isolation of pyrrolidine-d_n (n = 0−2). By this method, quantitative $^{13}C\{^1H\}$ NMR spectroscopy and mass spectrometric analysis established the presence of pyrrolidine (50%), pyrrolidine-2-d_1 (40%), pyrrolidine-2,5-d_1,d_1 (8%) and pyrrolidine-2-d_2 (2%) by comparison of the acquired spectrum to those of independently synthesized pyrrolidine isotopologues (Figure 4c; for syntheses of pyrrolidine isotopologues, see the Supporting Information). Control experiments involving addition of DCl to $[\mathbf{1\text{-}N(pyrr)}]^+$ ruled out modification of the isotopic content of the pyrrolidide ligand backbone as a result of treatment with acid. These results establish that $[\mathbf{1\text{-}N(pyrr\text{-}}d_n\mathbf{)}]^+$ contains α-(d_0−d_2) isotopologues at the pyrrolidide ligand, including two distinct d_2 isotopomers. The mechanistic significance of these isotopologues is discussed below.

Experiments were conducted to examine the effect of added phosphine as well as the reversibility of both the deuterium scrambling and H_2 evolution processes. Addition of 10 equiv of PPh_2Me to $[\mathbf{1\text{-}NH(pyrr)}]^+$ inhibited the dehydrogenation reaction with ∼10% diamagnetic $[\mathbf{1\text{-}N(pyrr)}]^+$ observed after heating at 60 °C after 1 day and ∼30% after 4 days. EPR spectroscopic analysis established $[\mathbf{1\text{-}NH(pyrr)}]^+$ as the sole paramagnetic compound during the course of this experiment, demonstrating that 10 equiv of added phosphine does not decompose the starting material. Addition of 4 atm of D_2 to $[\mathbf{1\text{-}N(pyrr)}]^+$ produced no detectable quantities of $[\mathbf{1\text{-}N(pyrr\text{-}}d_n\mathbf{)}]^+$ after 60 °C of heating at 5 days. These data suggest that phosphine dissociation is likely necessary for the observed N−H/D bond activation/H_2 evolution reactivity and that the overall H_2 evolution reaction is irreversible.

The relative time scales of hydrogen evolution and pyrrolidide ligand deuteration in $[\mathbf{1\text{-}N(pyrr\text{-}}d_n\mathbf{)}]^+$ were explored next. Observation of an isotopic perturbation of resonances in the pyrrolidide β-carbon signals in $[\mathbf{1\text{-}N(pyrr\text{-}}d_n\mathbf{)}]^+$ (Figure 4b) provided a convenient spectroscopic handle for probing the degree of pyrrolidide deuteration over the course of the dehydrogenation reaction. Accordingly, monitoring the relative areas of isotopically shifted β-pyrrolidine carbon signals in $[\mathbf{1\text{-}N(pyrr\text{-}}d_n\mathbf{)}]^+$ (26.75−26.51 ppm) by quantitative ^{13}C NMR spectroscopy established that the ratio d_0:(d_1 + d_2) pyrrolidide isotopologues remained constant over the course of the dehydrogenation of $[\mathbf{1\text{-}ND(pyrr)}]^+$ (3−48 h, 60 °C), indicating that pyrrolidide ligand deuteration proceeds more rapidly than $[\mathbf{1\text{-}N(pyrr\text{-}}d_n\mathbf{)}]^+$ formation. To eliminate the possibility that the deuterium label in pyrrolidine-1-d_1 scrambles rapidly upon coordination, a large excess (50 equiv) of PPh_2Me was added to $[\mathbf{1\text{-}ND(pyrr)}]^+$ to displace the pyrrolidine ligand, which enabled probing of its isotopic composition at various stages of the dehydrogenation reaction. Accordingly, $[\mathbf{1\text{-}ND(pyrr)}]^+$ was treated with 50 equiv of PPh_2Me and heated for 6 h at 60 °C, after which time a new paramagnetic molybdenum complex was formed, as judged by EPR spectroscopy (g_{iso} = 2.011, Figure S23), tentatively assigned as the cationic terpyridine tris(diphenylmethylphosphine) molybdenum complex $[(^{Ph}Tpy)(PPh_2Me)_3Mo][BArF^{24}]$ ($[\mathbf{1\text{-}PPh_2Me}]^+$) (Scheme 3, top). Concurrently,

Scheme 3. Displacement of the Pyrrolidine Ligand in $[\mathbf{1\text{-}ND(pyrr)}]^+$ at Various Time Intervals

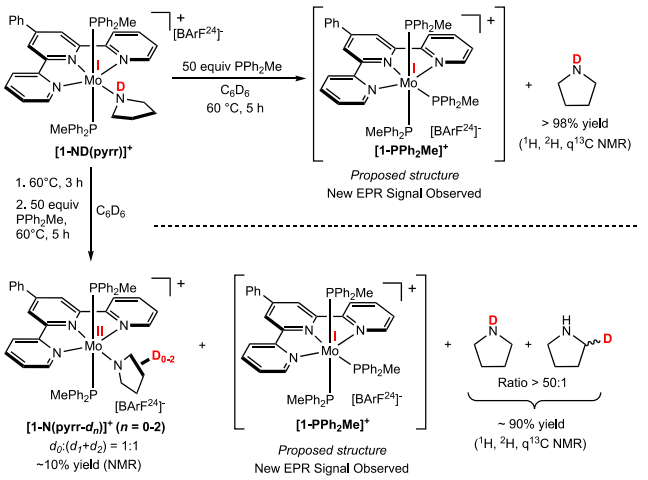

pyrrolidine-1-d_1 was detected as the exclusive diamagnetic product by quantitative $^{13}C\{^1H\}$ and ^2H NMR spectroscopy, demonstrating that deuterium incorporation into the pyrrolidine backbone in $[\mathbf{1\text{-}ND(pyrr)}]^+$ does not take place upon coordination to molybdenum at room temperature. Instead, the deuterium scrambling processes are likely tied to both H_2 evolution and $[\mathbf{1\text{-}N(pyrr\text{-}}d_n\mathbf{)}]^+$ formation that proceed upon thermolysis.

Next, the deuterium distribution in the pyrrolidine ligand at an early thermolysis stage was examined to probe the reversibility of the N−H/D activation reaction. Accordingly, the pyrrolidine dehydrogenation reaction was carried out to partial conversion (60 °C, 3 h, ∼10% conversion) followed by displacement of the pyrrolidine ligand by addition of a large excess of PPh_2Me (50 equiv). Only traces (<2%) of the α-deuterated pyrrolidine were observed by quantitative $^{13}C\{^1H\}$ NMR spectroscopy with the observation of predominantly pyrrolidine-1-d_1 (Scheme 3, bottom). This is in contrast to the observation of significant deuterium incorporation into the pyrrolidide ligand of the dehydrogenation product $[\mathbf{1\text{-}N(pyrr\text{-}}d_n\mathbf{)}]^+$ at an identical time point, with a d_0:(d_1 + d_2) pyrrolidide isotopologue ratio of ∼1:1 in $[(\mathbf{1\text{-}N(pyrr\text{-}}d_n\mathbf{)}]^+$ observed after 3 h at 60 °C (Scheme 3, bottom). When they are taken together, these data suggest that N−H/D activation in

https://dx.doi.org/10.1021/acs.organomet.0c00471
Organometallics XXXX, XXX, XXX−XXX

coordinated pyrrolidine in [**1-ND(pyrr)**]$^+$ is likely irreversible and that deuterium incorporation into the pyrrolidide ligand necessarily accompanies formation of the product [**1-N(pyrr-d_n)**]$^+$.

To probe whether the H_2 evolution reaction is intramolecular in nature, a key crossover experiment was conducted wherein [**1-NH(pyrr)**]$^+$ and [**1-ND(pyrr)**]$^+$ were mixed in a 1:1 ratio and heated in benzene solution at 60 °C for 48 h (Scheme 4).[49] The evolved gases were collected, analyzed, and

Scheme 4. Crossover Experiment between [1-NH(pyrr)]$^+$ and [1-ND(pyrr)]$^+$ and Subsequent Pyrrolidide Ligand Liberation by Protonolysis

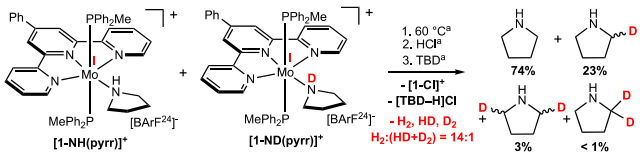

[a]For the reaction conditions, see the Supporting Information.

found to contain H_2 and HD + D_2 in a 14:1 ratio. The pyrrolidide ligand was liberated at the conclusion of the reaction by the protonolysis procedure described previously and found to contain pyrrolidine (74%), pyrrolidine-2-d_1 (23%), pyrrolidine-2,5-d_1,d_1 (3%), and pyrrolidine-2-d_2 (<1%). Because the relative percentages of H_2 and pyrrolidine isotopologues are approximately half of the values observed in the dehydrogenation of [**1-ND(pyrr)**]$^+$ where no [**1-NH(pyrr)**]$^+$ was added, these results demonstrate no deuterium crossover and support intramolecular deuterium scrambling and H_2 evolution pathways.

Proposed H_2 Evolution Pathway in Amine Complexes with Weak Bonds. A proposed H_2 evolution pathway that is consistent with the experimental results is presented in Scheme 5. Following phosphine dissociation, N–H(D) oxidative

Scheme 5. Proposed H_2 Evolution Pathway and Pyrrolidide Ligand Deuterium Incorporation Resulting in Formation of [1-N(pyrr-d_1)]$^+$

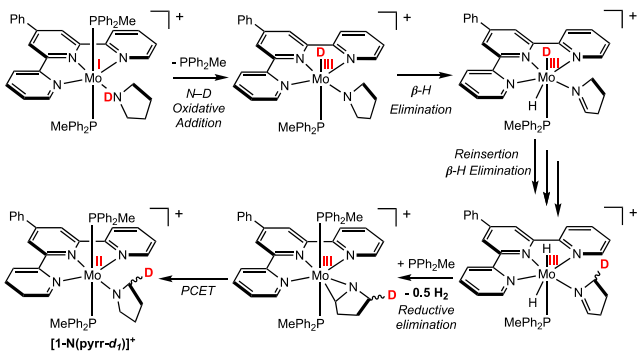

addition takes place and is followed by pyrrolidide β-H elimination[50,51] and reinsertion processes that account for scrambling of the deuterium label principally into the pyrrolidide 2- and 5-positions. No deuterium incorporation was observed in the pyrrolidide 3- and 4-positions of the product, suggesting that deuterium scrambling does not involve "chain walking" in the proposed imine intermediate. Intramolecular H_2 evolution proceeds by reductive elimination from a putative molybdenum dihydride imine intermediate. The resulting molybdenum azametallacyclopropane complex then undergoes an irreversible, bimolecular PCET reaction with the molybdenum(I) pyrrolidine starting material or any of the preceding intermediates with weak Mo–H bonds to generate the molybdenum(II) pyrrolidide product and accounts for the generation of pyrrolidide-d_2 isotopomers when the reaction involves N–D or Mo–D bonds (see below for computational evidence for low Mo(III)–H BDFEs). This step likely proceeds in analogy to the reported reactivity of [**1-NH$_3$**]$^+$ undergoing reductive PCET to the related molybdenum imido and ethylene complexes [**1-(N*t*BuAr)**]$^+$ and [**1-(C_2H_4)**]$^+$ to furnish [**1-NH$_2$**]$^+$ as well as the aryl amido and ethyl complexes [**1-(NH*t*BuAr)**]$^+$ and [**1-(CH_2CH_3)**]$^+$, respectively.[26,27] It is important to note that an intermolecular PCET event must occur to account for the net 1H$^+$/1e$^-$ change between the S = 1/2 [**1-NH(pyrr)**]$^+$ starting material and S = 0 [**1-N(pyrr)**]$^+$ product. However, deuterium scrambling and H_2 evolution likely precede product-forming PCET to account for the observation of constant pyrrolidide isotopologue ratios in [**1-N(pyrr-d_n)**]$^+$ as a function of reaction progress as well as the low deuterium content in the evolved gases.

While the pathway proposed in Scheme 5 accounts for the fate of the majority (~80%) of the deuterium label in the pyrrolidide ligand and evolved gases, ^{2}H NMR spectroscopy revealed a minor amount of deuterium incorporation both into *o*-phenyl (~6%) and methyl (~6%) positions of the PPh_2Me ligands in [**1-N(pyrr-d_n)**]$^+$ (Figure S5). Although the low deuterium content in the PPh_2Me ligands prevented identification of specific isotopomers and isotopologues by quantitative ^{13}C NMR spectroscopy, these results suggest that a minor phosphine ligand deuteration pathway is operative but is likely less facile than N–H/D bond activation upon thermolysis of [**1-ND(pyrr)**]$^+$ (Scheme S1).

The insights gained from the isotopic labeling experiments provide context for the H_2 evolution reaction in the nonclassical ammine complex [**1-NH$_3$**]$^+$. A key experimental connection between the ammine and pyrrolidine systems is the similarly nonstatistical amount of HD observed when [**1-NH$_3$**]$^+$ and [**1-ND$_3$**]$^+$ are mixed in a 1:1 ratio and heated (H_2:HD = 9:1),[25] suggestive of an intramolecular H_2 evolution mechanism. In analogy to [**1-NH(pyrr)**]$^+$, Scheme 6 presents a proposed pathway for [**1-NH$_3$**]$^+$ that involves an intramolecular H_2 evolution step and an intermolecular product-forming PCET reaction. Computational analysis of the BDFEs

Scheme 6. Proposed H_2 Evolution Pathway in [1-NH$_3$]$^+$ and DFT-Computed NH/Mo–H BDFEs of Intermediates at the B3LYP Level of Theory

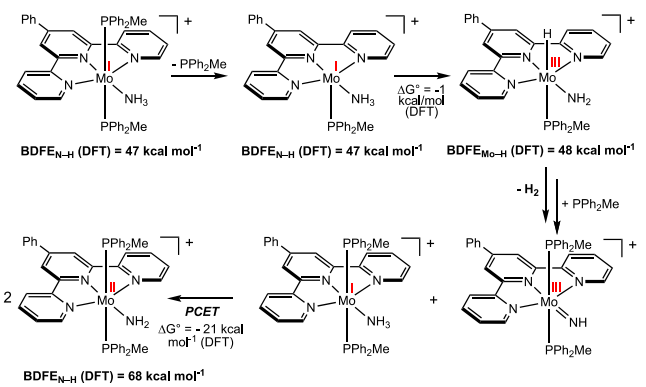

https://dx.doi.org/10.1021/acs.organomet.0c00471
Organometallics XXXX, XXX, XXX–XXX

of the intermediates demonstrates that phosphine dissociation does not have a significant effect on the ammine N−H BDFE, wherein an approximately thermoneutral N−H oxidative addition event ($\Delta G^\circ \approx -1$ kcal mol^{-1}) generates a proposed molybdenum amido hydride intermediate with a weak Mo−H BDFE of 48 kcal mol^{-1}, near the thermodynamic threshold for H_2 evolution. This is likely a key feature of these molybdenum complexes, as exergonic ammonia N−H oxidative addition would generate a strong M−H bond from which H_2 elimination is expected to be highly endergonic.[52] Key literature precedent for the subsequent 1,2-H_2 elimination step is Wolczanski's observation of H_2 evolution from $(silox)_3Ta(NH_2)(H)$ (silox = tBu_3SiO), a complex that was prepared by oxidative addition of ammonia.[53]

The final step of the pathway in Scheme 6 is intermolecular PCET between the starting ammine complex $[\mathbf{1}\text{-}\mathbf{NH_3}]^+$ and the proposed "parent" imido intermediate $[\mathbf{1{=}NH}]^+$ to generate 2 equiv of the amido product $[\mathbf{1}\text{-}\mathbf{NH_2}]^+$. This PCET step is predicted to be exergonic by 21 kcal mol^{-1}, driven by coordination-induced bond weakening in $[\mathbf{1}\text{-}\mathbf{NH_3}]^+$ ($BDFE_{N-H}$ = 47 kcal mol^{-1}) relative to the amido N−H bond formed ($BDFE_{N-H}$ = 68 kcal mol^{-1}). As mentioned previously, this step has direct precedent in that our group demonstrated that the aryl imido complex $[\mathbf{1}\text{-}(\mathbf{N}t\mathbf{BuAr})]^+$ reacts with $[\mathbf{1}\text{-}\mathbf{NH_3}]^+$ to generate the corresponding amido complexes $[\mathbf{1}\text{-}(\mathbf{NH}t\mathbf{BuAr})]^+$ and $[\mathbf{1}\text{-}\mathbf{NH_2}]^+$, a reaction that was shown to have a lower overall driving force in comparison to the reaction involving a "parent" amido.[26] In contrast to H_2 evolution, the PCET reactivity of $[\mathbf{1}\text{-}\mathbf{NH_3}]^+$ has been previously found to proceed independently of added phosphine[26,27] and is therefore proposed to take place between bis(phosphine) molybdenum complexes in Scheme 6. Because multiple intermediates in Scheme 6 were computed to contain weak (<50 kcal mol^{-1}) N−H and Mo−H bonds, PCET from these complexes to the parent imido is also thermodynamically feasible. Also important to note is that the proposed pathway can be generalized to account for the observation of H_2 evolution upon coordination of water and hydrazine to the cationic terpyridine bis(phosphine) molybdenum complex reported in our original study,[25] each likely proceeding through formally Mo(III) oxo and hydrazido intermediates, respectively.

Overall, the proposed mechanism presented is consistent with our originally reported crossover experiment whereby a 1:1 mixture of $[\mathbf{1}\text{-}\mathbf{NH_3}]^+$ and $[\mathbf{1}\text{-}\mathbf{ND_3}]^+$ were heated and a nonstatistical amount of HD gas was observed,[25] likely due to the intramolecular H_2 evolution step shown in Scheme 6. A recent computational study by Bandeira et al. on $[\mathbf{1}\text{-}\mathbf{NH_3}]^+$ is noteworthy and establishes the kinetic feasibility of ammonia N−H oxidative addition to yield a seven-coordinate Mo(III) amido hydride complex.[54] However, pathways involving phosphine dissociation and imido formation were not reported. While the possibility of phosphine dissociation taking place subsequent to N−H bond activation cannot be rigorously excluded, the experimental data support a unimolecular H_2 evolution pathway. In addition, it is worth noting that the proposed pathways in Schemes 5 and 6 represent a combination of classical organometallic steps as well as PCET enabled by coordination-induced bond weakening during H_2 evolution, likely a unique feature of cationic terpyridine bis(phosphine) molybdenum complexes.

CONCLUDING REMARKS

The synthesis and characterization of the cationic molybdenum pyrrolidine complex $[\mathbf{1}\text{-}\mathbf{NH}(\mathbf{pyrr})]^+$ supported by terpyridine and bis(phosphine) ligands are described. Significant weakening of the pyrrolidine N−H bond was demonstrated upon coordination to the molybdenum center that enables spontaneous H_2 evolution reactivity, with the N−H BDFE in $[\mathbf{1}\text{-}\mathbf{NH}(\mathbf{pyrr})]^+$ being experimentally determined to be in the range 41−51 kcal mol^{-1}. These findings are supported by the DFT-computed value of 48 kcal mol^{-1}. Deuterium labeling experiments were conducted, and the results support a dehydrogenation mechanism involving intramolecular H_2 evolution at a single molybdenum site followed by a product-forming intermolecular PCET reaction.

These investigations have examined the H_2-evolution reactivity of coordinated amines exhibiting exceptionally weak N−H bonds that may compete with PCET in the presence of H atom acceptors. Specifically, the coordinatively saturated complexes $[\mathbf{1}\text{-}\mathbf{NH_3}]^+$ and $[\mathbf{1}\text{-}\mathbf{NH}(\mathbf{pyrr})]^+$ behave as thermodynamically potent reductive PCET reagents similar to $(\eta^5\text{-}C_5H_5)_2TiCl(THF_x/H_2O_y)$ and $SmI_2(H_2O)_n$, whereby phosphine dissociation is the likely gateway to the observed dehydrogenation reactivity. While the phenomenon of coordination-induced bond weakening provides the overall thermodynamic driving force for H−H bond formation, it is likely the access to molybdenum hydride intermediates with low Mo−H BDFEs that opens the kinetic pathway for H_2 evolution upon phosphine dissociation. These insights will aid the application of coordination-induced bond weakening for the synthesis of complexes with exceptionally weak bonds, both in settings where H_2 evolution reactivity may be desirable and for cases where it is to be avoided.

ASSOCIATED CONTENT

Supporting Information

The Supporting Information is available free of charge at https://pubs.acs.org/doi/10.1021/acs.organomet.0c00471.

DFT-computed coordinates of complexes (XYZ)

General considerations, preparation of molybdenum complexes, characterization data including NMR and EPR spectra of complexes, electrochemical data, independent synthesis of pyrrolidine isotopologues and corresponding NMR spectra, deuterium labeling experiments and associated data, and computational methods and results (PDF)

AUTHOR INFORMATION

Corresponding Author

Paul J. Chirik − *Department of Chemistry, Princeton University, Princeton, New Jersey 08544, United States;* orcid.org/0000-0001-8473-2898; Email: pchirik@princeton.edu

Authors

Máté J. Bezdek − *Department of Chemistry, Princeton University, Princeton, New Jersey 08544, United States;* orcid.org/0000-0001-7860-2894

István Pelczer − *Department of Chemistry, Princeton University, Princeton, New Jersey 08544, United States;* orcid.org/0000-0002-7806-6101

Complete contact information is available at: https://pubs.acs.org/10.1021/acs.organomet.0c00471

https://dx.doi.org/10.1021/acs.organomet.0c00471
Organometallics XXXX, XXX, XXX−XXX

Notes

The authors declare no competing financial interest.

■ ACKNOWLEDGMENTS

Financial support was provided by the U.S. Department of Energy, Office of Science, Basic Energy Science (DE-SC0006498). M.J.B. thanks the Natural Sciences and Engineering Research Council of Canada for a predoctoral fellowship (PGS-D) and Princeton University for a Porter Ogden Jacobus Honorific Fellowship. We thank Ken Conover (Princeton University) for assistance with the acquisition of quantitative ^{13}C-NMR spectra.

■ REFERENCES

(1) Warren, J. J.; Tronic, T. A.; Mayer, J. M. Thermochemistry of Proton-Coupled Electron Transfer Reagents and its Implications. *Chem. Rev.* **2010**, *110*, 6961−7001.
(2) Huynh, M. H. V.; Meyer, T. J. Proton-Coupled Electron Transfer. *Chem. Rev.* **2007**, *107*, 5004−5064.
(3) Hammes-Schiffer, S. Introduction: Proton-Coupled Electron Transfer. *Chem. Rev.* **2010**, *110*, 6937−6938.
(4) Mayer, J. M. Understanding Hydrogen Atom Transfer: From Bond Strengths to Marcus Theory. *Acc. Chem. Res.* **2011**, *44*, 36−46.
(5) Reece, S. Y.; Nocera, D. G. Proton-Coupled Electron Transfer in Biology: Results from Synergistic Studies in Natural and Model Systems. *Annu. Rev. Biochem.* **2009**, *78*, 673−699.
(6) Dempsey, J. L.; Winkler, J. R.; Gray, H. B. Proton-Coupled Electron Flow in Protein Redox Machines. *Chem. Rev.* **2010**, *110*, 7024−7039.
(7) Hoffman, B. M.; Dean, D. R.; Seefeldt, L. C. Climbing Nitrogenase: Toward a Mechanism of Enzymatic Nitrogen Fixation. *Acc. Chem. Res.* **2009**, *42*, 609−619.
(8) Miller, D. C.; Tarantino, K. T.; Knowles, R. R. Proton-Coupled Electron Transfer in Organic Synthesis: Fundamentals, Applications, and Opportunities. *Top. Curr. Chem.* **2016**, *374*, 30.
(9) Crossley, S. W. M.; Obradors, C.; Martinez, R. M.; Shenvi, R. A. Mn-, Fe-, and Co-Catalyzed Radical Hydrofunctionalization of Olefins. *Chem. Rev.* **2016**, *116*, 8912−9000.
(10) Cook, T. R.; Dogutan, D. K.; Reece, S. Y.; Surendranath, Y.; Teets, T. S.; Nocera, D. G. Solar Energy Supply and Storage for the Legacy and Nonlegacy Worlds. *Chem. Rev.* **2010**, *110*, 6474−6502.
(11) Gagliardi, C. J.; Vannucci, A. K.; Concepcion, J. J.; Chen, Z.; Meyer, T. J. The Role of Proton Coupled Electron Transfer in Water Oxidation. *Energy Environ. Sci.* **2012**, *5*, 7704−7717.
(12) Blakemore, J. D.; Crabtree, R. H.; Brudvig, G. W. Molecular Catalysts for Water Oxidation. *Chem. Rev.* **2015**, *115*, 12974−13005.
(13) For selected experimental studies on aquo, hydroxo, amine, amide and imide ligand bond dissociation enthalpies (BDEs) and BDFEs in metal complexes, see: (a) Binstead, R. A.; Moyer, B. A.; Samuels, G. J.; Meyer, T. J. Proton-coupled electron transfer between $[Ru(bpy)_2(py)OH_2]^{2+}$ and $[Ru(bpy)_2(py)O]^{2+}$. A solvent isotope effect (k_{H2O}/k_{D2O}) of 16.1. *J. Am. Chem. Soc.* **1981**, *103*, 2897−2899. (b) Jonas, R. T.; Stack, T. D. P. C−H Bond Activation by a Ferric Methoxide Complex: A Model for the Rate-Determining Step in the Mechanism of Lipoxygenase. *J. Am. Chem. Soc.* **1997**, *119*, 8566−8567. (c) Larsen, A. S.; Wang, K.; Lockwood, M. A.; Rice, G. L.; Won, T.-J.; Lovell, S.; Sadílek, M.; Tureek, F.; Mayer, J. M. Hydrocarbon Oxidation by Bis-μ-oxo Manganese Dimers: Electron Transfer, Hydride Transfer, and Hydrogen Atom Transfer Mechanisms. *J. Am. Chem. Soc.* **2002**, *124*, 10112−10123. (d) Gupta, R.; Borovik, A. S. Monomeric $Mn^{III/II}$ and $Fe^{III/II}$ Complexes with Terminal Hydroxo and Oxo Ligands: Probing Reactivity via O−H Bond Dissociation Energies. *J. Am. Chem. Soc.* **2003**, *125*, 13234−13242. (e) De Angelis, F.; Jin, N.; Car, R.; Groves, J. T. Electronic Structure and Reactivity of Isomeric Oxo-Mn(V) Porphyrins: Effects of Spin State Crossing and pK_a Modulation. *Inorg. Chem.* **2006**, *45*, 4268−4276. (f) Rittle, J.; Green, M. T. Cytochrome P450 compound I: capture, characterization, and C-H bond activation kinetics. *Science* **2010**, *330*, 933−937. (g) Donoghue, P. J.; Tehranchi, J.; Cramer, C. J.; Sarangi, R.; Solomon, E. I.; Tolman, W. B. Rapid C−H Bond Activation by a Monocopper(III)−Hydroxide Complex. *J. Am. Chem. Soc.* **2011**, *133*, 17602. (h) Leung, S. K.-Y.; Tsui, W.-M.; Huang, J.-S.; Che, C.-M.; Liang, J.-L.; Zhu, N. Imido Transfer from Bis(imido)ruthenium(VI) Porphyrins to Hydrocarbons: Effect of Imido Substituents, C−H Bond Dissociation Energies, and $Ru^{VI/V}$ reduction potentials. *J. Am. Chem. Soc.* **2005**, *127*, 16629−16640. (i) Eckert, N. A.; Vaddadi, S.; Stoian, S.; Lachicotte, R. J.; Cundari, T. R.; Holland, P. L. Coordination-Number Dependence of Reactivity in an Imidoiron(III) Complex. *Angew. Chem., Int. Ed.* **2006**, *45*, 6868−6871. (j) Tarantino, K. T.; Miller, D. C.; Callon, T. A.; Knowles, R. R. Bond-Weakening Catalysis: Conjugate Aminations Enabled by the Soft Homolysis of Strong N−H Bonds. *J. Am. Chem. Soc.* **2015**, *137*, 6440−6443. (k) Pappas, I.; Chirik, P. J. Ammonia Synthesis by Hydrogenolysis of Titanium−Nitrogen Bonds Using Proton Coupled Electron Transfer. *J. Am. Chem. Soc.* **2015**, *137*, 3498−3501. (l) Scheibel, M. G.; Abbenseth, J.; Kinauer, M.; Heinemann, F. W.; Würtele, C.; de Bruin, B.; Schneider, S. Homolytic N−H Activation of Ammonia: Hydrogen Transfer of Parent Iridium Ammine, Amide, Imide, and Nitride Species. *Inorg. Chem.* **2015**, *54*, 9290−9302. (m) Lindley, B. M.; Bruch, Q. J.; White, P. S.; Hasanayn, F.; Miller, A. J. M. Ammonia Synthesis from a Pincer Ruthenium Nitride via Metal-Ligand Cooperative Proton-Coupled Electron Transfer. *J. Am. Chem. Soc.* **2017**, *139*, 5305−5308. (n) Reed, C. J.; Agapie, T. Thermodynamics of Proton and Electron Transfer in Tetranuclear Clusters with Mn−OH_2/OH Motifs Relevant to H_2O Activation by the Oxygen Evolving Complex in Photosystem II. *J. Am. Chem. Soc.* **2018**, *140*, 10900−10908. (o) Resa, S.; Millán, A.; Fuentes, N.; Crovetto, L.; Marcos, M. L.; Lezama, L.; Choquesillo-Lazarte, D.; Blanco, V.; Campaña, A. G.; Cárdenas, D. J.; Cuerva, J. M. O−H and (CO)N−H bond weakening by coordination to Fe(II). *Dalton Trans.* **2019**, *48*, 2179−2189. (p) Kadassery, K. J.; Sethi, K.; Fanara, P. M.; Lacy, D. C. CO-Photolysis-Induced H-Atom Transfer from Mn^{I}O−H Bonds. *Inorg. Chem.* **2019**, *58*, 4679−4685. (q) Bruch, Q. J.; Connor, G. P.; Chen, C.-H.; Holland, P. L.; Mayer, J. M.; Hasanayn, F.; Miller, A. J. M. Dinitrogen Reduction to Ammonia at Rhenium Utilizing Light and Proton-Coupled Electron Transfer. *J. Am. Chem. Soc.* **2019**, *141*, 20198−20208.
(14) For selected experimental studies on X−H (X = N, O) BDEs and BDFEs at remote positions in chelating ligands in metal complexes, see: (a) Roth, J. P.; Lovell, S.; Mayer, J. M. Intrinsic Barriers for Electron and Hydrogen Atom Transfer Reactions of Biomimetic Iron Complexes. *J. Am. Chem. Soc.* **2000**, *122*, 5486−5498. (b) Yoder, J. C.; Roth, J. P.; Gussenhoven, E. M.; Larsen, A. S.; Mayer, J. M. Electron and Hydrogen-Atom Self-Exchange Reactions of Iron and Cobalt Coordination Complexes. *J. Am. Chem. Soc.* **2003**, *125*, 2629−2640. (c) Roth, J. P.; Yoder, J. C.; Won, T.-J.; Mayer, J. M. Application of the Marcus Cross Relation to Hydrogen Atom Transfer Reactions. *Science* **2001**, *294*, 2524−2526. (d) Manner, V. W.; Mayer, J. M. Concerted Proton−Electron Transfer in a Ruthenium Terpyridyl-Benzoate System with a Large Separation between the Redox and Basic Sites. *J. Am. Chem. Soc.* **2009**, *131*, 9874−9875.
(15) For selected experimental studies on ligand C−H BDEs and BDFEs in metal complexes, see: (a) Kerr, M. E.; Zhang, X.-M.; Bruno, J. W. Effects of the Niobium(V) Center on the Energetics of Ligand-Centered Proton and Hydrogen Atom Transfer Reactions in Acyl and Alkoxide Complexes. *Organometallics* **1997**, *16*, 3249. (b) Zhang, S. Z.; Bordwell, F. G. Effects of π-Coordinated Transition-Metal Groups on Fluorene Acidities and Homolytic Bond Dissociation Enthalpies. *Organometallics* **1994**, *13*, 2920−2921. (c) Trujillo, H. A.; Casado, C. M.; Ruiz, J.; Astruc, D. Thermodynamics of C−H Activation in Multiple Oxidation States: Comparison of Benzylic C−H Acidities and C−H Bond Dissociation Energies in the Isostructural 16−20-Electron Complexes $[Fe^{x}(\eta^5\text{-}C_5R_5)(\eta^6\text{-arene})]^{n}$, x = 0−IV, R = H or Me, n = − 1 to + 3. *J. Am. Chem. Soc.* **1999**, *121*, 5674−5686. (d) Trujillo, H. A.; Casado, C. M.; Astruc, D. Thermodynamics of Benzylic C-H Activation in 18- and 19-Electron Iron Sandwich

https://dx.doi.org/10.1021/acs.organomet.0c00471
Organometallics XXXX, XXX, XXX−XXX

Complexes: Determination of pK_a values and Bond Dissociation Energies. *J. Chem. Soc., Chem. Commun.* **1995**, 7−8. (e) Semproni, S. P.; Milsmann, C.; Chirik, P. J. Four-Coordinate Cobalt Pincer Complexes: Electronic Structure Studies and Ligand Modification by Homolytic and Heterolytic Pathways. *J. Am. Chem. Soc.* **2014**, *136*, 9211−9224. (f) Chalkley, M. J.; Oyala, P. H.; Peters, J. C. Cp* Noninnocence Leads to a Remarkably Weak C−H Bond via Metallocene Protonation. *J. Am. Chem. Soc.* **2019**, *141*, 4721−4729.

(16) For selected reviews on and examples of studies experimentally examining metal−hydride BDEs and BDFEs, see: (a) Rakowski DuBois, M.; DuBois, D. L. The roles of the first and second coordination spheres in the design of molecular catalysts for H_2 production and oxidation. *Chem. Soc. Rev.* **2009**, *38*, 62−72. (b) Bullock, R. M. Metal-Hydrogen Bond Cleavage Reactions of Transition Metal Hydrides: Hydrogen Atom, Hydride, and Proton Transfer Reactions. *Comments Inorg. Chem.* **1991**, *12*, 1−33. (c) Eisenberg, D. C.; Norton, J. R. Hydrogen-Atom Transfer Reactions of Transition-Metal Hydrides. *Isr. J. Chem.* **1991**, *31*, 55−66. (d) Hu, Y.; Shaw, A. P.; Estes, D. P.; Norton, J. R. Transition-Metal Hydride Radical Cations. *Chem. Rev.* **2016**, *116*, 8427−8462. (e) Crossley, S. W. M.; Obradors, C.; Martinez, R. M.; Shenvi, R. A. Mn-, Fe-, and Co-Catalyzed Radical Hydrofunctionalizations of Olefins. *Chem. Rev.* **2016**, *116*, 8912−9000. (f) Fu, X.; Wayland, B. B. Thermodynamics of Rhodium Hydride Reactions with CO, Aldehydes, and Olefins in Water: Organo Rhodium Porphyrin Bond Dissociation Free Energies. *J. Am. Chem. Soc.* **2005**, *127*, 16460−16467. (g) Cui, W.; Wayland, B. B. Activation of C−H/H−H Bonds by Rhodium(II) Porphyrin Bimetalloradicals. *J. Am. Chem. Soc.* **2004**, *126*, 8266−8274.

(17) For selected experimental studies on ligand P−H BDEs in metal complexes, see: (a) Buss, J. A.; Hirahara, M.; Ueda, Y.; Agapie, T. Molecular Mimics of Heterogeneous Metal Phosphides: Thermochemistry, Hydride-Proton Isomerism, and HER Reactivity. *Angew. Chem., Int. Ed.* **2018**, *57*, 16329−16333. (b) Abbenseth, J.; Delony, D.; Neben, M. C.; Würtele, C.; de Bruin, B.; Schneider, S. Interconversion of Phosphinyl Radical and Phosphinidene Complexes by Proton Coupled Electron Transfer. *Angew. Chem., Int. Ed.* **2019**, *58*, 6338−6341.

(18) Bordwell, F. G.; Bausch, M. J. Acidity-Oxidation-Potential (AOP) Values as Estimates of Relative Bond Dissociation Energies and Radical Stabilities in Dimethyl Sulfoxide Solution. *J. Am. Chem. Soc.* **1986**, *108*, 1979−1985.

(19) Cuerva, J. M.; Campana, A. G.; Justicia, J.; Rosales, A.; Oller-Lopez, J. L.; Robles, R.; Cardenas, D. J.; Bunuel, E.; Oltra, J. E. Water: The Ideal Hydrogen-Atom Source in Free-Radical Chemistry Mediated by Ti^{III} and Other Single-Electron-Transfer Metals? *Angew. Chem., Int. Ed.* **2006**, *45*, 5522−5526.

(20) Paradas, M.; Campaña, A. G.; Jimenez, T.; Robles, R.; Oltra, J. E.; Buñuel, E.; Justicia, J.; Cárdenas, D. J.; Cuerva, J. M. Understanding the Exceptional Hydrogen-Atom Donor Characteristics of Water in Ti^{III}-Mediated Free-Radical Chemistry. *J. Am. Chem. Soc.* **2010**, *132*, 12748−12756.

(21) Gansäuer, A.; Behlendorf, M.; Cangönül, A.; Kube, C.; Cuerva, J. M.; Friedrich, J.; van Gastel, M. H_2O Activation for Hydrogen-Atom Transfer: Correct Structures and Revised Mechanisms. *Angew. Chem., Int. Ed.* **2012**, *51*, 3266−3270.

(22) Chciuk, T. V.; Flowers, R. A. Proton-Coupled Electron Transfer in the Reduction of Arenes by SmI_2−Water Complexes. *J. Am. Chem. Soc.* **2015**, *137*, 11526−11531.

(23) Kolmar, S. S.; Mayer, J. M. $SmI_2(H_2O)_n$ reduction of electron rich enamines by proton-coupled electron transfer. *J. Am. Chem. Soc.* **2017**, *139*, 10687−10692.

(24) Ashida, Y.; Arashiba, K.; Nakajima, K.; Nishibayashi, Y. Molybdenum-catalysed ammonia production with samarium diiodide and alcohols or water. *Nature* **2019**, *568*, 536−540.

(25) Bezdek, M. J.; Guo, S.; Chirik, P. J. Coordination-induced weakening of ammonia, water, and hydrazine X−H bonds in a molybdenum complex. *Science* **2016**, *354*, 730−733.

(26) Bezdek, M. J.; Chirik, P. J. Interconversion of Molybdenum Imido and Amido Complexes by Proton−Coupled Electron Transfer. *Angew. Chem., Int. Ed.* **2018**, *57*, 2224−2228.

(27) Bezdek, M. J.; Chirik, P. J. Proton−Coupled Electron Transfer to a Molybdenum Ethylene Complex Yields a β-Agostic Ethyl: Structure, Dynamics and Mechanism. *J. Am. Chem. Soc.* **2018**, *140*, 13817−13826.

(28) Ishitani, O.; White, P. S.; Meyer, T. J. Formation of Dinitrogen by Oxidation of $[(bpy)_2(NH_3)RuORu(NH_3)(bpy)_2]^{4+}$. *Inorg. Chem.* **1996**, *35*, 2167−2168.

(29) Klerke, A.; Christensen, C. H.; Nørskov, J. K.; Vegge, T. Ammonia for hydrogen storage: challenges and opportunities. *J. Mater. Chem.* **2008**, *18*, 2304−2310.

(30) Margulieux, G. W.; Turner, Z. R.; Chirik, P. J. Synthesis and Ligand Modification Chemistry of a Molybdenum Dinitrogen Complex: Redox and Chemical Activity of a Bis(imino)pyridine Ligand. *Angew. Chem., Int. Ed.* **2014**, *53*, 14211−14215.

(31) Keener, M.; Peterson, M.; Hernández-Sánchez, R.; Oswald, V. F.; Wu, G.; Ménard, G. Towards Catalytic Ammonia Oxidation to Dinitrogen: A Synthetic Cycle by Using a Simple Manganese Complex. *Chem. - Eur. J.* **2017**, *23*, 11479−11484.

(32) Habibzadeh, F.; Miller, S. L.; Hamann, T. W.; Smith, M. R. Homogeneous electrocatalytic oxidation of ammonia to N_2 under mild conditions. *Proc. Natl. Acad. Sci. U. S. A.* **2019**, *116*, 2849−2853.

(33) Zott, M. D.; Garrido-Barros, P.; Peters, J. C. Electrocatalytic Ammonia Oxidation Mediated by a Polypyridyl Iron Catalyst. *ACS Catal.* **2019**, *9*, 10101−10108.

(34) Bhattacharya, P.; Heiden, Z. M.; Chambers, G. M.; Johnson, S. I.; Bullock, R. M.; Mock, M. T. Catalytic Ammonia Oxidation to Dinitrogen by Hydrogen Atom Abstraction. *Angew. Chem., Int. Ed.* **2019**, *58*, 11618−11624.

(35) Nakajima, K.; Toda, H.; Sakata, K.; Nishibayashi, Y. Ruthenium-catalysed oxidative conversion of ammonia into dinitrogen. *Nat. Chem.* **2019**, *11*, 702−709.

(36) Dunn, P. L.; Johnson, S. I.; Kaminsky, W.; Bullock, R. M. Diversion of Catalytic C−N Bond Formation to Catalytic Oxidation of NH_3 through Modification of the Hydrogen Atom Abstractor. *J. Am. Chem. Soc.* **2020**, *142*, 3361−3365.

(37) Gunanathan, C.; Milstein, D. Bond Activation and Catalysis by Ruthenium Pincer Complexes. *Chem. Rev.* **2014**, *114*, 12024−12087.

(38) Dub, P. A.; Henson, N. J.; Martin, R. L.; Gordon, J. C. Unravelling the Mechanism of the Asymmetric Hydrogenation of Acetophenone by $[RuX_2(diphosphine)(1,2\text{-diamine})]$ Catalysts. *J. Am. Chem. Soc.* **2014**, *136*, 3505−3521.

(39) Dub, P. A.; Matsunami, A.; Kuwata, S.; Kayaki, Y. Cleavage of N−H Bond of Ammonia via Metal−Ligand Cooperation Enables Rational Design of a Conceptually New Noyori−Ikariya Catalyst. *J. Am. Chem. Soc.* **2019**, *141*, 2661−2677.

(40) Bezdek, M. J.; Guo, S.; Chirik, P. J. Terpyridine Molybdenum Dinitrogen Chemistry: Synthesis of Dinitrogen Complexes That Vary by Five Oxidation States. *Inorg. Chem.* **2016**, *55*, 3117−3127.

(41) Mader, E. A.; Manner, V. W.; Markle, T. F.; Wu, A.; Franz, J. A.; Mayer, J. M. Trends in Ground-State Entropies for Transition Metal Based Hydrogen Atom Transfer Reactions. *J. Am. Chem. Soc.* **2009**, *131*, 4335−4345.

(42) The dehydrogenation reaction also took place in a closed system at room temperature over the course of an extended time period (ca. 1−2 weeks), arguing against an entropy-driven H_2 evolution process at elevated temperatures.

(43) Elgrishi, N.; Kurtz, D. A.; Dempsey, J. L. Reaction Parameters Influencing Cobalt Hydride Formation Kinetics: Implications for Benchmarking H_2-Evolution Catalysts. *J. Am. Chem. Soc.* **2017**, *139*, 239−244.

(44) Savéant, J.-M. *Elements of Molecular and Biomolecular Electrochemistry*; Wiley: Hoboken, NJ, 2006.

(45) Kaljurand, I.; Rodima, T.; Pihl, A.; Mäemets, V.; Leito, I.; Koppel, I. A.; Mishima, M. Acid−Base Equilibria in Nonpolar Media. 4. Extension of the Self-Consistent Basicity Scale in THF Medium.

https://dx.doi.org/10.1021/acs.organomet.0c00471
Organometallics XXXX, XXX, XXX−XXX

Gas-Phase Basicities of Phosphazenes. *J. Org. Chem.* **2003**, *68*, 9988−9993.
(46) A more accurate definition for this lower bound is complicated by the dearth of reagents with higher known pK_a values in THF that do not decompose [**1-N(pyrr)**]$^+$.
(47) Assuming C_G = 60.4 kcal mol^{-1} in THF. Concerning this constant, see: Wise, C. F.; Agarwal, R. G.; Mayer, J. M. Determining Proton-Coupled Standard Potentials and X−H Bond Dissociation Free Energies in Nonaqueous Solvents Using Open-Circuit Potential Measurements. *J. Am. Chem. Soc.* **2020**, *142*, 10681−10691.
(48) We note that the electrochemical conditions used in the present study (in particular, the identity of the supporting electrolyte) differ from those employed for the determination of C_G in ref 47, which may introduce error (ca. ±2 kcal mol^{-1}) in the estimate of this lower bound.
(49) Reaction completeness was judged by quantitative ^{13}C NMR spectroscopy.
(50) For an example of *β*-H elimination from an amido ligand of molybdenum, see: Tsai, Y.-C.; Johnson, M. J. A.; Mindiola, D. J.; Cummins, C. C.; Klooster, W. T.; Koetzle, T. F. A Cyclometalated Resting State for a Reactive Molybdenum Amide: Favorable Consequences of *β*-Hydrogen Elimination Including Reductive Cleavage, Coupling, and Complexation. *J. Am. Chem. Soc.* **1999**, *121*, 10426−10427.
(51) For conceptually analogous *β*-H elimination reactions involving alkoxide ligands, see: Blum, O.; Milstein, D. Mechanism of a Directly Observed *β*-Hydride Elimination Process of Iridium Alkoxo Complexes. *J. Am. Chem. Soc.* **1995**, *117*, 4582−4594.
(52) Macgregor, S. A. Theoretical Study of the Oxidative Addition of Ammonia to Various Unsaturated Low-Valent Transition Metal Species. *Organometallics* **2001**, *20*, 1860−1874.
(53) Hulley, E. B.; Bonanno, J. B.; Wolczanski, P. T.; Cundari, T. R.; Lobkovsky, E. B. Pnictogen-Hydride Activation by $(silox)_3Ta$ (silox = tBu_3SiO); Attempts to Circumvent the Constraints of Orbital Symmetry in N_2 Activation. *Inorg. Chem.* **2010**, *49*, 8524−8544.
(54) Bandeira, N. A. G.; Veiros, L. F.; Bo, C. Hydrogen Generation via Activation of X−H Bonds in Ammonia and Water by an Mo^I Complex. *ChemistrySelect* **2017**, *2*, 11071−11082.

https://dx.doi.org/10.1021/acs.organomet.0c00471
Organometallics XXXX, XXX, XXX−XXX